biophysica

MDPI

Article

Temperature Distribution and Control in Ultrasound-Based Therapy: An Ex Vivo Study with Bioheat Transfer Modeling

Ali Dahaghin [1,*], Milad Salimibani [2,*] and Paria Jahansa [3]

[1] Department of Anthropology, Hirszfeld Institute of Immunology and Experimental Therapy, Polish Academy of Sciences, 53-114 Wrocław, Poland
[2] Department of Optics and Photonics, Wroclaw University of Science and Technology, 50-370 Wrocław, Poland
[3] Department of Psychology, Carl von Ossietzky Universität Oldenburg, 26129 Oldenburg, Germany
* Correspondence: ali.dahaghin@hirszfeld.pl (A.D.); milad.salimibani@pwr.edu.pl (M.S.)

Abstract

In therapeutic applications, ultrasound is widely used in physiotherapy, tissue repair, and cancer treatment. Regarding cancer treatment, as an emerging field for technology, significant research efforts have been devoted to the area of ultrasound therapy. The derived energy from beams can be deposited in tissues not only through heating but also through non-thermal mechanisms, whereby cancer cells are subject to cell death. Ultrasound-induced heating can generate localized temperature elevations within biological tissues, making it a subject of interest for thermal therapeutic applications. Nevertheless, excessive temperature elevations outside the primary exposure region may result in undesirable thermal effects within the surrounding tissue. In this study, we used continuous 3 MHz ultrasound waves at the powers of 0.4 to 1.4 W on ex vivo chicken breast tissue in a water bath to prevent fluctuations in temperature. The process was also numerically modeled with a maximum error of 0.4% from the measured data. Temperature measurements revealed a significant difference between the region of maximum acoustic pressure along the beam axis and deeper tissue locations (in some cases, above 3.5 °C). These findings indicate that temperature gradients can develop within homogeneous tissue during ultrasound exposure, emphasizing the importance of controlling acoustic power and exposure conditions. Moreover, increasing the temperature was significant during the first moments of treatment, which highlights the importance of precise controls for rate and precision in therapy. The numerical simulations also showed that increasing acoustic power elevates tissue temperature while simultaneously producing a less uniform temperature distribution. These observations may be useful for the optimization of future ultrasound-based thermal treatment strategies; however, direct clinical extrapolation requires further investigation using physiologically representative tissue models.

Keywords: ultrasound; hyperthermia; thermal damage; numerical modeling; cancer therapy

Check for updates

Academic Editor: Dragan Nikolic

Received: 17 April 2026
Revised: 15 June 2026
Accepted: 16 June 2026
Published: 25 June 2026

Copyright: © 2026 by the authors. Licensee MDPI, Basel, Switzerland. This article is an open access article distributed under the terms and conditions of the Creative Commons Attribution (CC BY) license.

1. Introduction

From the therapeutic view, a treatment plan with accurate estimation of heat deposition, which is performed during the least possible time, is pivotal in achieving an effective clinical outcome. Hyperthermia treatment planning (HTP) is crucial to improving locoregional heating and the final outcomes in ultrasound therapy. Effective HTP requires careful selection of an optimal treatment technique, as well as an accurate calculation of

power deposition and temperature distribution in the patient body [1]. Recent advances in HTP has placed value on hyperthermia in a broad range of medical applications, as ultrasound opens up the possibility of reaching deep and hard-to-access tissues [2]. Therapeutic ultrasound [3], which has been used in physiotherapy practices for many years, is used to provide deep heating to soft tissues in the human body, as well as non-thermal effects, where high-frequency ultrasound waves cause dislocation and movement of cellular fluids. These tissues include muscles, tendons, joints, and ligaments. Ultrasound can be employed to improve lesions, heal fractured bones, reduce muscle spasms, treat joint stiffness, increase flexibility in tendons and ligaments, and boost nerve conduction velocity [4–7]. In lithotripsy, focused ultrasound waves are directly sent to the stone to break it into smaller stones that will eventually pass through the urinary tract [8]. Moreover, especially in recent years, the advent of the drug delivery system has opened a new area of application for ultrasound therapy [9,10]. New drug/gene delivery systems have been a focus of interest in, especially in cancer treatments, as the full range of designed delivery systems provides a various set of advantages [11]. High-frequency waves of ultrasounds are employed in various drug/gene delivery systems to promote drug delivery to the brain, as they are able to transiently and locally open the blood–brain barrier [12,13]. Ultrasound-guided drug/gene delivery in cancer has attracted much attention, with an increasing number of studies employing the technique. In cancer treatment, a great deal of interest in ultrasound therapy is caused by the accurate targeting of the intended tissues without damaging healthy cells [14,15]. The importance of finding brand-new solutions in cancer cures with minimized toxicity to healthy tissues cannot be overstated. Hence, ultrasound therapy can be a promising tool in the field. Up to this day, this approach has been employed in a wide range of tumors [16,17], including renal [18], prostate [19], liver [20], breast [21], pancreatic [22], and uterine cancer [23]. High-intensity focused ultrasound (HIFU) is a treatment that aims to target and kill cancer cells [24]. Safety and control of unwanted damage to the healthy cells are integral with HIFU; thus, a trend in the on-going research on HIFU is to find the optimum HTP to provide the best possible clinical outcomes with minimized side effects [25]. The use of nanoparticles is a complement to this treatment [26]. In physical therapy, it was proven that only a 1 °C increase in tissue temperature raises metabolic activity. Further increase up to 2–3 °C is associated with relief in muscle spasms and rigidity. In contrast, 4 °C could eventually lead to an improvement in the flexibility of the collagen compartment of muscle [5]. Concomitant with radiotherapy and chemotherapy, hyperthermia can be used for a better clinical outcome in cancer therapy. This approach has been performed for many years in treating progressed tumors. As supported by a considerable number of preclinical and clinical trials, hyperthermia combination therapy can significantly contribute to the effective treatment of cancer, indicating the role of thermal therapy as an adjuvant to the conventional treatments. In the range of 41 °C to 45 °C, immune systems become active, boosting the anti-cancer activity of the conventional treatments [27]. When the temperature rises up to 55 °C, a direct effect on the cancer tissue induces coagulated necrosis in the cancer tissue [28]. In brief, regarding the heating plan, hyperthermia can be divided into (1) thermal ablation (46 °C $\leq T \leq$ 56 °C), (2) moderate hyperthermia (41 °C $\leq T \leq$ 46 °C), and (3) diathermia (T $\leq$ 41 °C) [29,30]. Local heating of tumors with the least damage to the surrounding tissues can be achieved using ultrasound. As mentioned, the optimum hyperthermia therapy is maximized damage to the cancer cells with the minimized side effects of off-targeting healthy tissues. This can be achieved using the HIFU technique; nevertheless, unwanted side effects might be inevitable in many cases. Treatment with HIFU might lead to local pain, bleeding, infection, swelling, burns, and blistering [31], as well as non-thermal adverse effects, including, as the most important one, cavitation, which increases the risk of tumor vessel rupture, hemorrhage, and metas-

tasis. Fast expansion and collapse of cavitation bubbles can quickly cause high pressure and extend the thermal effects [32,33]. Thus, precise control of the factors impacting the hyperthermia process is pivotal to successful therapy. These factors include but are not limited to frequency, depth of the tissue, tissue type, ultrasound intensity, and the area being treated [5,34].

Consequently, in effective ultrasound therapy, the following statements must be considered [35]:

(1) Accurate location of the targeted tissue.
(2) Anticipating the possible thermal adverse effects on the area being treated.
(3) Real-time observation and control of the whole process, with considerable attention to the detrimental effects on healthy tissues.
(4) Monitoring the biological changes as a marker for the efficacy of treatment.

As noted previously, one of the biggest challenges in ultrasound therapy is the evaluation of the thermal load on tissue and the likely adverse effects on the surrounding tissues [36,37]. At present, magnetic resonance imaging (MRI) is one of the popular modalities in hyperthermia treatment. For this aim, measuring temperature changes during hyperthermia treatment can be achieved by magnetic resonance thermometry using the proton resonance frequency shift method. However, due to the frequency drift of the MRI system, significant errors with the measured temperature change hinder the exact thermal evaluation. Another method is signal processing using ultrasound waves, but as in MRI, this method is rather costly for thermal evaluation and might not be feasible in clinical application [38]. The rise in temperature depends on the ultrasound source parameters, tissue properties, and shape of the beam [39]. The third option for temperature monitoring is thermocouples. These cheap and easy-to-use electric devices have repeatedly appeared in numerous studies on thermal evaluation. Although thermocouples are invasive thermometers, they are favored for ex vivo studies [40]. This paper aims to evaluate the temperature gradients resulting from different distances between the ultrasound probe and targeted tissue, using 3 MHz ultrasound waves at various powers of the transducer. We attempted to monitor temperature directly in the targeted area and its border with surrounding tissues and record the fluctuation in heating to prevent possible thermal damage to the surrounding tissue areas. The entire process can also be modeled in order to improve the treatment planning [41]. Here, we used COMSOL Multiphysics to simulate wave propagation followed by heat generation in the tissue, which showed an excellent agreement between the numerical results and the experimental data.

2. Materials and Methods

2.1. Material

The study was conducted at the department of medical physics' laboratory at the Iran University of Medical Sciences (IUMS). For temperature monitoring, two thermocouples (Hanyoung®, Korea, 125 µm diameter sheath, accuracy of 0.1 °C) were used, and for ultrasound therapy, the Phyaction (190i, Germany) was used with continuous 1:1 pulsations (0.4–1.4 W/cm^2 at 3 MHz). The ultrasound probe was flat and non-focused (head size of 1 cm^2). Ultrasound waves of 1–5 MHz are used for HIFU therapeutic application [42]; thus, in this research, we set the frequency at 3 MHz. Eighteen fresh slices of chicken breast were used for the experiments. The chicken breast samples were obtained fresh from a local supplier on the same day as the experiments and were stored under refrigerated conditions at approximately 4 °C prior to use. Before the experiments, the samples were removed from refrigeration and maintained at room temperature for approximately 3 h to achieve thermal equilibrium. No chemical preservation or dehydration procedures were applied to the tissues before measurements. Although the hydration levels of the samples were not

quantified, efforts were made to minimize tissue dehydration during sample preparation and experimentation by maintaining the tissues within a water-containing experimental setup. The slices were cubic (40 ± 1 mm) and left at room temperature (21 °C) 3 h before the experiments. All experiments were conducted in a temperature-controlled laboratory environment. The ambient room temperature was maintained at 21 ± 1 °C throughout all measurements using the laboratory's air-conditioning system. Although relative humidity was not actively controlled, it remained within the laboratory's normal operating range during the experiments. To minimize external thermal disturbances, all measurements were performed away from direct sunlight and external heat-generating equipment. In addition, tissue samples were immersed in a water bath with an initial temperature of approximately 21 °C to reduce rapid environmental temperature fluctuations and improve thermal stability. No active temperature-controlled systems, water circulation, or mechanical agitation were employed during the experiments; therefore, small local temperature variations may have occurred during ultrasound exposure. To keep the structure of the chicken breast slices stable, the pieces were cut with a polycarbonate mold (cube No. 1, 40 ± 1 mm) and were put in a bigger cube mold filled with water (21 °C) (cube No. 2, 126.6 ±1 mm) (Figure 1). During the experiment, the water temperature was constant with the room temperature. At the bottom of each cube, an acoustic wave-absorbing layer was placed to reduce ultrasound reflections within the experimental setup. The absorber consisted of a commercially available soft rubber-based damping material, with an approximate thickness of 10 mm. Although the exact acoustic impedance and absorption coefficient of the material were not experimentally measured, the material was selected due to its high attenuation characteristics and its common use for minimizing acoustic reflections in laboratory ultrasound experiments.

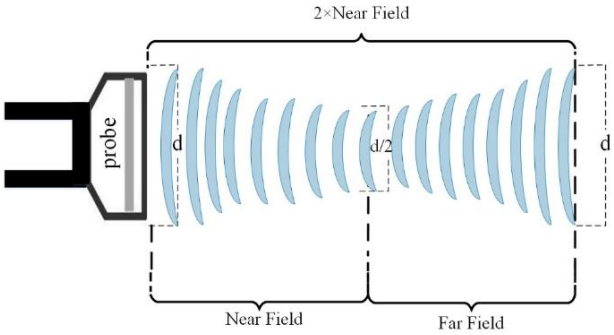


Figure 1. Illustration of the near-field, Fresnel, and Fraunhofer regions of a linear probe, with d as the probe diameter.

2.2. Experimental Setup

At first, the ultrasound remains cylindrical along the path of the beam axis, which is aligned perpendicular to the center of the crystal. However, after some distance, as shown in (Figure 2), the beam starts to converge and then diverge. The region before the beam divergence area is referred to as the Fresnel zone, and the beam divergence region as the Fraunhofer zone [43,44].

Near-zone length is derived from Equation (1) [45]:

$$\text{Near} - \text{zone length} = \frac{diameter^2}{4 \times \lambda} \quad (1)$$

Wavelength is designated by the Greek letter lambda (λ), as given by Equation (2) [43]:

$$\lambda = \frac{C}{f}, \quad (2)$$

where C is the speed of sound (m/s) and f is the wave's frequency measured in the MHz unit. Given the probe area of 1 cm^2:

$$\pi r^2 = 1 \text{ cm}^2 \text{ where } r = 5.64 \text{ mm}$$

The most crucial point derived from the speed of sound in different tissues is that, regardless of tissue type, the speed of sound in soft tissues is approximately the same. As per the method in this study, 3 MHz ultrasound waves were used to travel through two different environments of water and chicken breast, and the waves travel most of the way in the water. According to the data, between the speed of sound in water (1484 m/s) [46] and chicken breast (1533 m/s) [47], there is only 3.3% difference; therefore, to simplify the calculation, water is considered as the whole environment of the experiment. Hence, near-zone length is measured as follows:

$$\text{Near} - \text{zone length} = \frac{diameter^2}{4 \times \lambda} = \frac{r^2}{\lambda} = \frac{r^2 f}{c} = \frac{\left(5.6 \times 10^{-3}\right)^2 \times 3 \times 10^6}{1484} = 63.3 \text{ mm}$$

where r represents the radius of the ultrasound transducer. It should be noted that, for the flat unfocused transducer used in the present study, the acoustic field does not exhibit a true geometric focus as observed in focused HIFU systems. Instead, the ultrasound field is characterized by near-field interference patterns and pressure maxima along the beam axis within the Fresnel region. Therefore, the region discussed in this study corresponds to the location of maximum acoustic pressure in the near field rather than a sharply defined focal point. The beam narrowing within this region is associated with constructive interference effects and should not be interpreted as a true geometric focusing phenomenon [45]. In practical experimental conditions, the acoustic field distribution may be influenced by diffraction effects, edge waves, attenuation, and medium heterogeneity, particularly at the water–tissue interface. Moreover, the employed transducer was not a focused HIFU source and therefore did not generate a sharply localized focal region. Consequently, the calculated near-field length should be interpreted as an approximate estimation of the acoustic field behavior rather than an exact representation of the spatial pressure distribution. Nevertheless, the equation provides a useful first-order approximation for characterizing the propagation region of the flat transducer used in the present study. It should also be emphasized that the calculated near-field length of 63.3 mm represents a theoretical estimate derived from the analytical model and was not experimentally validated through acoustic field mapping. Consequently, this value should not be interpreted as the exact location of maximum acoustic pressure or temperature within the experimental setup.

With increasing the ultrasound intensity, the produced heat rises, but the location of the point where the temperature is at its maximum does not merely change, as it is more dependent on frequency and speed and rises with frequency [42]. The speed of sound relies on the density and elasticity of the media through which it is traveling. The following equation (Equation (3)) reflects these parameters:

$$c = \sqrt{\frac{\beta}{\rho}}, \tag{3}$$

where β is the coefficient of stiffness representing modulus of bulk elasticity (kg/m), and ρ is the density of the elastic medium (kg/m^3) [43].

According to Equation (3), rises in temperature could lead to density alteration, which in turn affects the speed of sound within the media. At the same time, changes in ultrasound speed, as per Equations (1) and (2), alter the focal area. Changes in these parameters and their effects in water are represented in Table 1 [48].

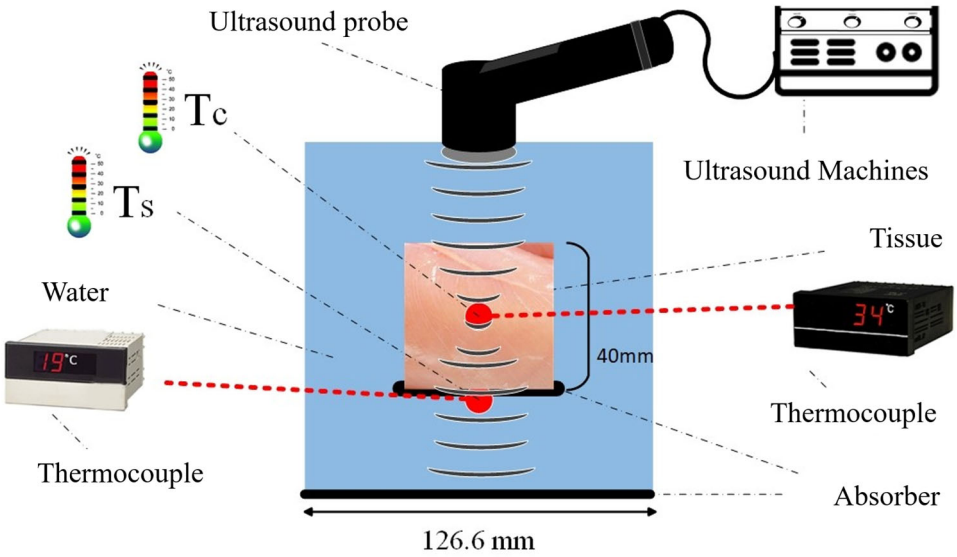


Figure 2. A schematic representation of the experiment showing the locations of the tissue, thermocouples, and ultrasound probe.

Table 1. Effects of water temperature variation on acoustic propagation parameters.

Change in Parameter	Value	%
Temperature	Less than 7 °C	-
Speed	Less than 27 m/s	Less than 1.8%
Near-zone length	Lest than −1.1 mm	Less than 1.7%

As mentioned in this section, the overall change in temperature in this study was no more than 7 °C; such temperature variations could lead to changes of less than approximately 1.8% in the speed of sound and less than approximately 1.7% in the estimated near-field length. These variations were considered relatively small compared with the overall uncertainties associated with the experimental and numerical setup and were therefore neglected to simplify the model. Consequently, near-field length and acoustic propagation parameters were assumed to remain approximately constant during simulations.

During ultrasound radiation, the temperature was measured in two areas. Both thermocouples were positioned along the central axis of the ultrasound beam (r = 0 mm). The T_C thermocouple was placed at the geometrical center of the cubic tissue sample, corresponding to approximately 20 mm below the upper tissue surface and 20 mm above the lower tissue surface. The T_S thermocouple was positioned at the lower central region of the tissue sample, adjacent to the lower tissue boundary, corresponding to 40 mm below the upper tissue surface (as shown in Figure 2).

(1) The temperature at the center of the tissue sample (hereafter referred to as T_C) was measured using a thermocouple positioned at the geometrical center of the sample. T_C represents the temperature measured at the central measurement location within the homogeneous tissue specimen.

(2) The temperature at the lower central region of the tissue sample (hereafter referred to as T_S) was measured using a second thermocouple positioned near the lower boundary of the specimen along the beam axis. T_S represents the temperature measured at a deeper location within the homogeneous tissue sample.

It should be noted that the present ex vivo model employed homogeneous chicken breast tissue and therefore does not reproduce the complex biological interface between tumor and healthy tissues observed in clinical conditions.

T_S is an important parameter, and its value is informed by the following three facts:

- The heat from the central part of the tissue increases its value.
- It represents the temperature of the surrounding parts of the tissues located along the direction of the waves; thus, it continuously rises as the ultrasound radiation proceeds.
- It is directly influenced by the immense heat transfer area (such as the water container in this study or internal organs and blood circulation in the human body).

Continuous 3 MHz exposure was used for each experiment. The temperature was recorded with thermocouples every 30 s for a total of 5 min. Experiments were performed on three different tissues and repeated three times. Six different acoustic power levels (0.4 to 1.4 W/cm^2, with 0.2 sequential increases) were investigated in the experiments. For each power level, measurements were performed using three independent chicken breast tissue samples, resulting in a total of 18 samples (40 $\pm$ 1 mm). Each tissue sample was used for only one experimental condition to avoid possible thermal history effects from previous ultrasound exposure.

2.3. Numerical Simulation

The numerical simulations were implemented in COMSOL Multiphysics 5.6 using a two-dimensional axisymmetric formulation. The pressure acoustics and frequency domain interface was employed to model ultrasound wave propagation, while the heat transfer in solids interface was used to simulate temperature evolution within the tissue and surrounding water media. Coupling between the acoustic and thermal problems was achieved through the acoustic heat source term derived from ultrasound attenuation.

The acoustic field was first solved in the frequency domain to obtain the spatial distribution of acoustic pressure. The resulting acoustic intensity distribution was subsequently introduced into the transient heat transfer model as a volumetric heat source. Time-dependent thermal simulations were then performed over a total duration of 5 min.

A direct solver was used in the simulations, with automatic time stepping implemented by COMSOL. The convergence criteria and relative tolerances were kept at the default COMSOL settings to ensure numerical stability and convergence of the coupled solution. The input parameters were considered to be exactly the same as the experiment (Tables 2 and 3).

Table 2. Chicken breast properties used in the simulation [49,50].

Parameter	Symbol	Value
Attenuation coefficient	α_0	5×10^{-8} (Np·Hz^{-1}·cm^{-1})
Density	ρ	1040 (kg·m^{-3})
Speed of sound	c	1533 (m·s^{-1})
Thermal conductivity	k	0.4683 (W·m^{-1}·C^{-1})
Specific heat capacity	C_p	3210 (J·kg^{-1}·C^{-1})

Table 3. Water properties used in the simulation [49].

Parameter	Symbol	Value
Attenuation coefficient	α_0	0.025 (Np·m^{-1})
Density	ρ	998 (kg·m^{-3})
Speed of sound	c	1484 (m·s^{-1})
Thermal conductivity	k	0.598 (W·m^{-1}·C^{-1})
Specific heat capacity	C_p	4182 (J·kg^{-1}·C^{-1})

2.4. Ultrasound Pressure

Ultrasound waves travel through media in the form of mechanical energy caused by the vibration of particles. Particles are also compressed and rarefied by wave propagation,

generating a pressure wave. At lower powers of the transducer, particle displacement is small and thus, it can be assumed that the wave propagation is linear [51]; therefore, the Helmholtz equation is used to describe the acoustic pressure as follows [52]:

$$\frac{\partial}{\partial r}\left[-\frac{r}{\rho_c}\left(\frac{\partial p}{\partial r}\right)\right]+r\frac{\partial}{\partial z}\left[-\frac{1}{\rho_c}\left(\frac{\partial p}{\partial z}\right)\right]-\left[\left(\frac{\omega}{c_c}\right)^2\right]\frac{rp}{\rho_c}=0, \tag{4}$$

where p is the acoustic pressure, ω is the angular frequency, and c_c and ρ_c are the complex speed of sound and complex density, respectively, which are defined as [53]:

$$c_c=\frac{\omega}{\left(\frac{\omega}{c}-i\alpha\right)}, \tag{5}$$

$$\rho_c=\frac{\rho c^2}{{c_c}^2}, \tag{6}$$

where ρ is the medium density, c is the speed of the sound in the medium, and α is the attenuation coefficient of the medium.

2.5. Heat Transfer

As the ultrasound waves penetrate into the tissue, attenuation of the energy occurs. This mechanical loss leads to temperature elevation [54]. The generated heat distribution can be modeled using the bioheat equation [55,56]:

$$\rho c_p\frac{\partial T}{\partial t}=\nabla\cdot(k\nabla T)+\rho_b c_b\omega_b(T_A-T)+Q_{met}+Q_{ext}, \tag{7}$$

where T is temperature, ρ is the density of the tissue, c is the specific heat capacity of the tissue, k is the thermal conductivity of the tissue, ρ_b is the density of blood, c_b is the specific heat capacity of blood, ω_b is the blood perfusion rate, T_A is the arterial temperature, Q_{met} is the metabolic heat generation rate of the tissue, and Q_{ext} is the acoustic heat source. However, in this study, as the experiments were carried out on a piece of chicken breast, the blood terms and metabolic heat source have been neglected. Therefore, the implemented model represents a simplified thermal conduction formulation with an ultrasound-induced acoustic heat source rather than the complete physiological Pennes bioheat model. Consequently, the thermal behavior obtained in this study primarily reflects conductive heat transfer combined with acoustic energy absorption under controlled laboratory conditions.

The acoustic heat source is defined by Equation (8) [51]:

$$Q_{ext}=2\alpha I, \tag{8}$$

where I is the acoustic intensity, as expressed by Equation (9):

$$I=\frac{p^2}{2\rho c}, \tag{9}$$

where p is the acoustic pressure obtained from the Helmholtz equation, ρ is the density of the medium, and c is the speed of sound in the medium.

Moreover, α is the frequency-dependent attenuation coefficient obtained from Equation (10) [57]:

$$\alpha=\alpha_0\left(\frac{f}{f_0}\right)^n, \tag{10}$$

where f_0 is 1 MHz and n is 1 for biological tissues and 2 for water. Values of α_0 for chicken breast and water are presented in Tables 2 and 3, respectively. Several studies have shown

that the attenuation coefficient of tissue may change during the experiment based on the temperature, heating duration, and type of tissue. However, it has also been indicated that the attenuation coefficient starts to increase at temperatures above 55 °C [58]. Therefore, the attenuation coefficient of tissue has an approximately constant value in hyperthermia temperature ranges.

2.6. Initial and Boundary Conditions

Ultrasound pressure at the beginning of the process was set to be zero, as there was no wave propagating through the domain at $t = 0$.

A flux boundary condition equal to $-\omega\Delta x^2$ was considered at the surface of the transducer, where ω is the frequency of the transducer and Δx is the normal displacement of the transducer, which is calculated using the equation below [17]:

$$\Delta x = \sqrt{\frac{P}{2S\pi^2 f^2 \rho_w c_w}}, \tag{11}$$

where P and S are the power and surface area of the transducer, respectively; f is the frequency at which the transducer operates; ρ_w is the density of water; and c_w is the speed of sound in water.

A perfectly matched layer (PML) was also regarded at the bottom of the bowl to act as an absorber of waves and prevent their reflection.

In order to prevent tissues from overheating, as mentioned before, the temperature of the water surrounding the tissue was set to 21 °C during the whole process as a simplifying boundary condition, and the initial temperature of the entire domain was considered to be 21 °C. Figure 3 illustrates a schematic of the geometry of the model and boundary conditions.

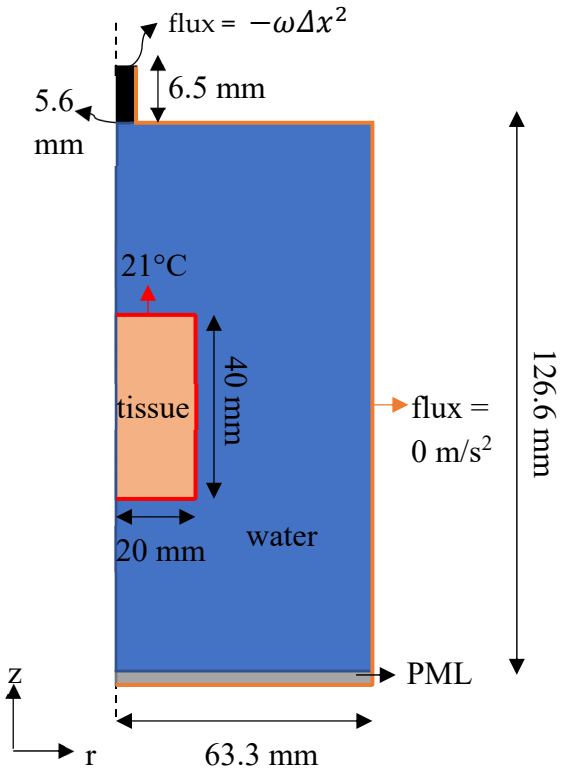


Figure 3. Schematic of the geometry of the model and boundary conditions.

2.7. Mesh Generation

A built-in quality assessment was used to evaluate the element quality [59]. Mesh distribution in acoustic pressure and heat transfer was considered to be the same. A free triangular mesh with a maximum element size of $\frac{c}{6f}$ at the water domain and $\frac{c}{8f}$ at the tissue was constructed. The size of the elements should be smaller than the wavelength of the acoustic waves; as the acoustic pressure at the tissue was of higher importance than at water in this study, more elements were built in this domain. Mapped mesh with the maximum element size of 1.5 mm was used for the perfectly matched layer domain. The number of the elements in this area was less than the other domains because acoustic waves do not penetrate into this region. Figure 4 shows the mesh distribution in the entire domain.

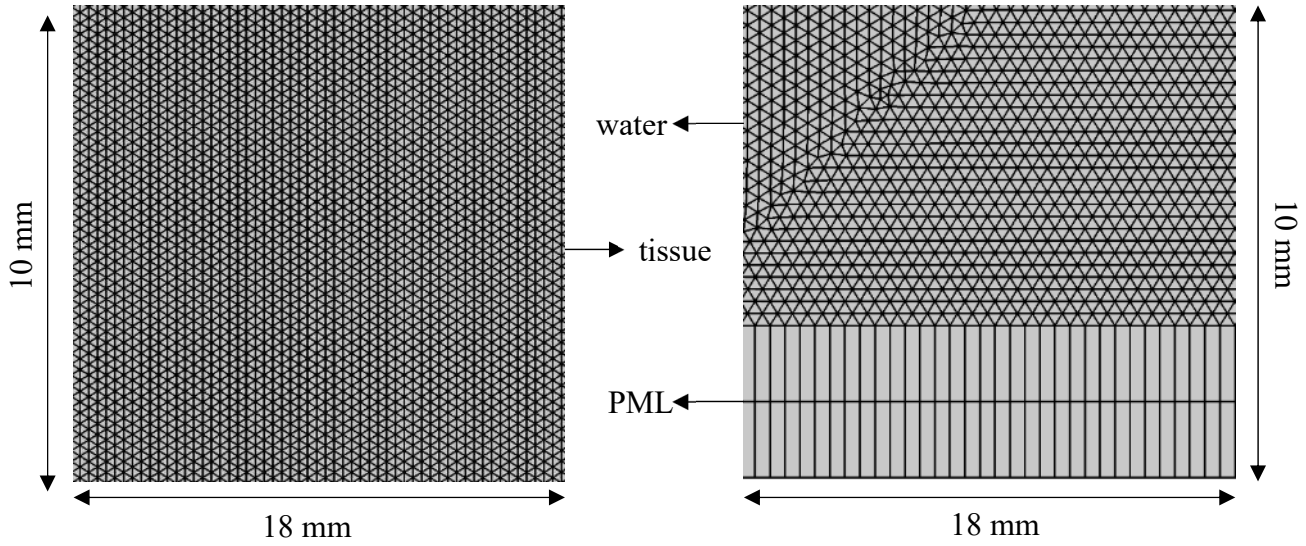


Figure 4. Mesh distribution within the tissue, water, and PML.

3. Results

T_C and T_S values were recorded every 30 s, followed by recorded rises in temperature at different time sets. An average of three results for every power (the probe area was 1 cm^2, so the intensity and power were equal) was measured and used as the final value for each sample. Afterward, the changes in temperature for different powers were plotted against the time points (Figure 5).

Previous studies have demonstrated that rises in temperature are often dependent on several factors, such as frequency, intensity, exposure time, and the intrinsic sensitivity of treated tissue to radiation in a non-linear behavior [60]. Our findings were also in agreement with previous works, as the relationship between the variables was non-linear and the obtained chart was somewhat radical.

According to the results, T_C always had a higher value than T_S, which was reasonably expected, as T_C represents the center temperature of the tissue. The results indicate that the rise in T_C was higher than it was in T_S, which is crucial to successful clinical hyperthermia as T_C corresponds to the targeted site. At the same time, T_S represents the possible damage to the healthy tissues and cells.

As shown in Figure 5, the rate of increase in temperature during the first 30 or 60 s is significantly higher than the other times, and the slope decreases with time. The decline in temperature rise approximately 1 min after exposure is due to the establishment of a heating balance between ultrasonic heating and tissue thermal conductivity [61]. Generally, for ultrasonic waves with frequencies higher than 1.5 MHz, the temperature reaches its balance rapidly, and the temperature changes slowly over time [42]. This points to the

importance of accuracy and speed during the first moments of radiation in therapeutic ultrasound applications. Due to the delicacy of different treatment methods, caution must be taken with the temperature rise in the beginning moments to reduce unwanted thermal damages [62].

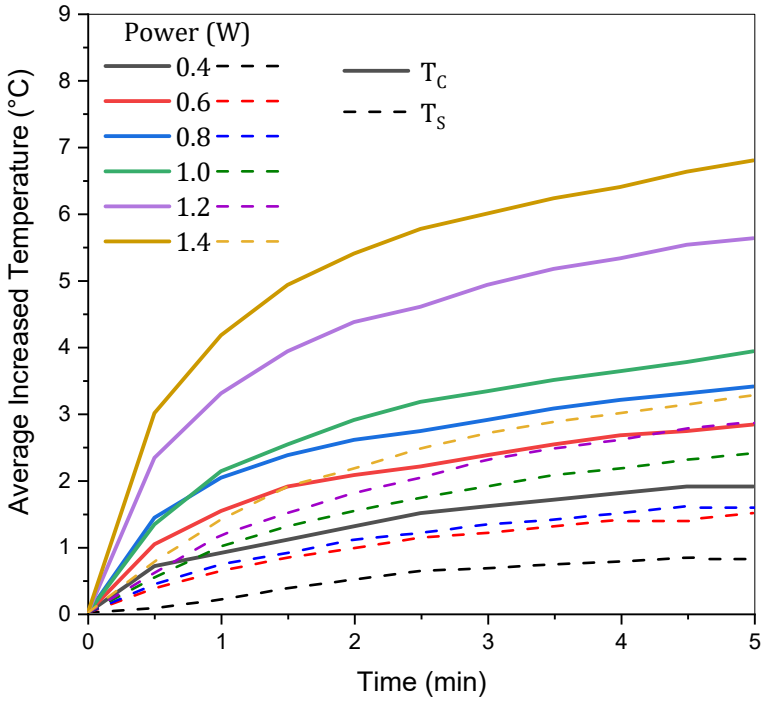


Figure 5. The increases in temperature with 3 MHz ultrasound beams with powers of 0.4–1.4 W at T_C and T_S.

The same scenario occurs for T_S increase as a function of time with some exceptions, as shown in Figure 5; although the first 30 or 60 s saw a steep rise in temperature similar to T_C, the slope of this increase had a lower amount. This observation can be explained by the fact that during the first minute, the dominant heating source was the direct exposure of the ultrasound beam, while in proceeding minutes, the established balance between ultrasonic heating and tissue thermal conduction reduced the slope of the ascending part of the temperature–time curve [61]. However, as the thermal transfer continued, the tissue center became a new source of energy that forced the chart to go up more rapidly for the following minutes, so the curve once again merely ascended to reach a new peak. The change in the temperature in this step was directly dependent on the convective heat transfer coefficient of the tissue [63]. For a better understanding of this result, a graph of temperature gradients based on time is presented in Figure 6. As can be seen, the gradients of fluctuations are very significant, especially in the first minute. After that, the increase in the temperature is slowed down by the cooling effect of the water surrounding the tissue, resulting in a gradual descent in the curve. This is pivotal in cancer therapy, as malignant tumor tissues in many cancers, such as lymphoma, bladder, colon, liver, breast, prostate, and spleen cancer, have a high conductive heat transfer coefficient, increasing the risk of adverse effects compared to the healthy tissues.

As per the results of the study, it is clear that regardless of wave's intensity, the temperature rises with ultrasound exposure time; as the intensity increases, the temperature–time slope increases, as we have the highest temperature rise at the power of 1.4 W. The results during the first 5 min are shown in Table 4. For completeness, the total temperature profiles for all investigated power levels are presented in the Supplementary Materials.

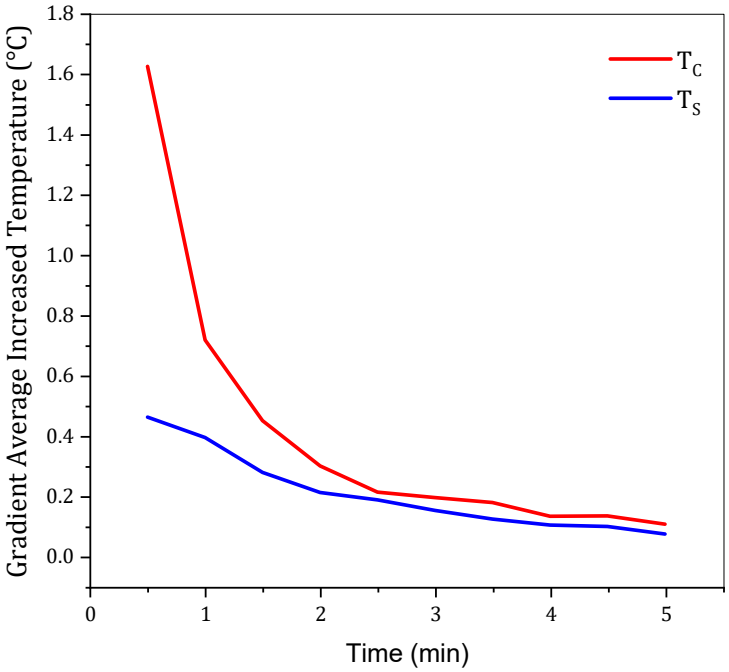


Figure 6. Graph of the T_C and T_S gradients.

Table 4. Rises in T_C and T_S values during the first 5 min of ultrasound therapy.

Power (W)	**0.4**	**0.6**	**0.8**	**1.0**	**1.2**	**1.4**
T_C	1.9	2.83	3.40	3.93	5.63	6.80
T_S	0.83	1.50	1.60	2.40	2.87	3.27

Figure 7 indicates the acoustic pressure field along the radial axis for various powers of the transducer at the end of the process. As can be seen, although increasing the power does not change the pressure field pattern, it increases the magnitude of the pressure field within the tissue. Maximum pressure amplitude within the tissue increased by 22%, 15%, 12%, 10%, and 8% when the power was raised from 0.4 to 0.6, 0.6 to 0.8, 0.8 to 1, 1 to 1.2, and 1.2 to 1.4, respectively (Figures 7 and 8). This finding is in agreement with Abdolhosseinzadeh's [53] findings, which showed that doubling the power from 5 W to 10 W increased the pressure amplitude from 0.91 MPa to 1.29 MPa. As one moves away from the *z*-axis, where the peak pressure occurs, variations in the pressure amplitude become less significant, meaning that the pressure profile becomes more uniform. Maximum pressure was achieved at 2 mm below the surface of the tissue along the *z*-axis at all powers, while maximum temperature was obtained at 9 mm below the upper boundary of the tissue at r = 0 due to the cooling effect of the surrounding water, which prevents overheating of the area near the surface of the tissue. The location of the point with the maximum temperature does not change with the acoustic power. Therefore, increasing the power cannot be effective if one wants to achieve the highest temperature at the center of the tissue. In fact, higher powers of the transducer result in higher temperatures. As the power increased, pressure distribution became less uniform, leading to a less uniform temperature distribution within the tissue, which could be attributed to the larger variations in the magnitude of the heat sources. Figure 9 showcase this best.

In order to determine how successful the numerical simulation can be in predicting the experimental results, time-dependent temperature of the center of the tissue was compared to that of the measured data (Figure 10). It can be seen that the curves follow the same trend, and the maximum relative percentage error of 0.4% confirms the accuracy of the

numerical simulation. The comparison was performed for all recorded time points during the 5 min exposure period.

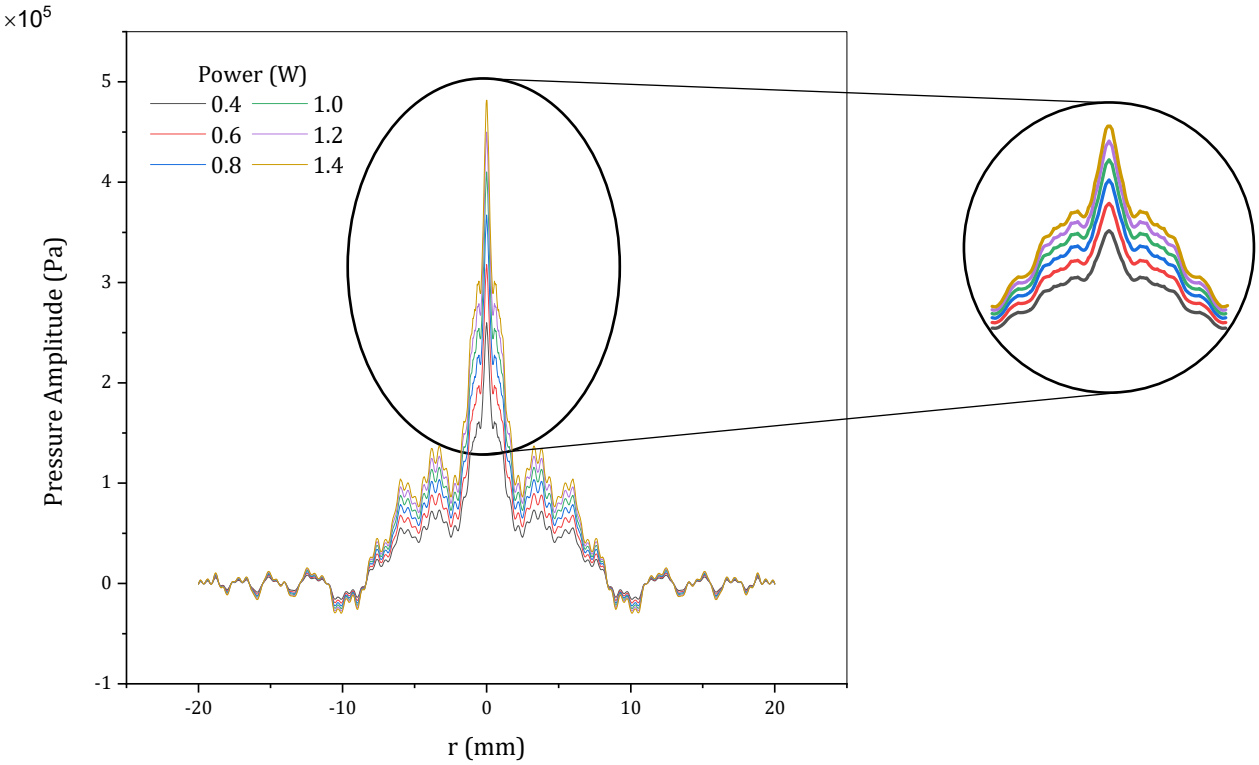


Figure 7. Pressure amplitude along the radial axis at various acoustic powers, obtained from the numerical model.

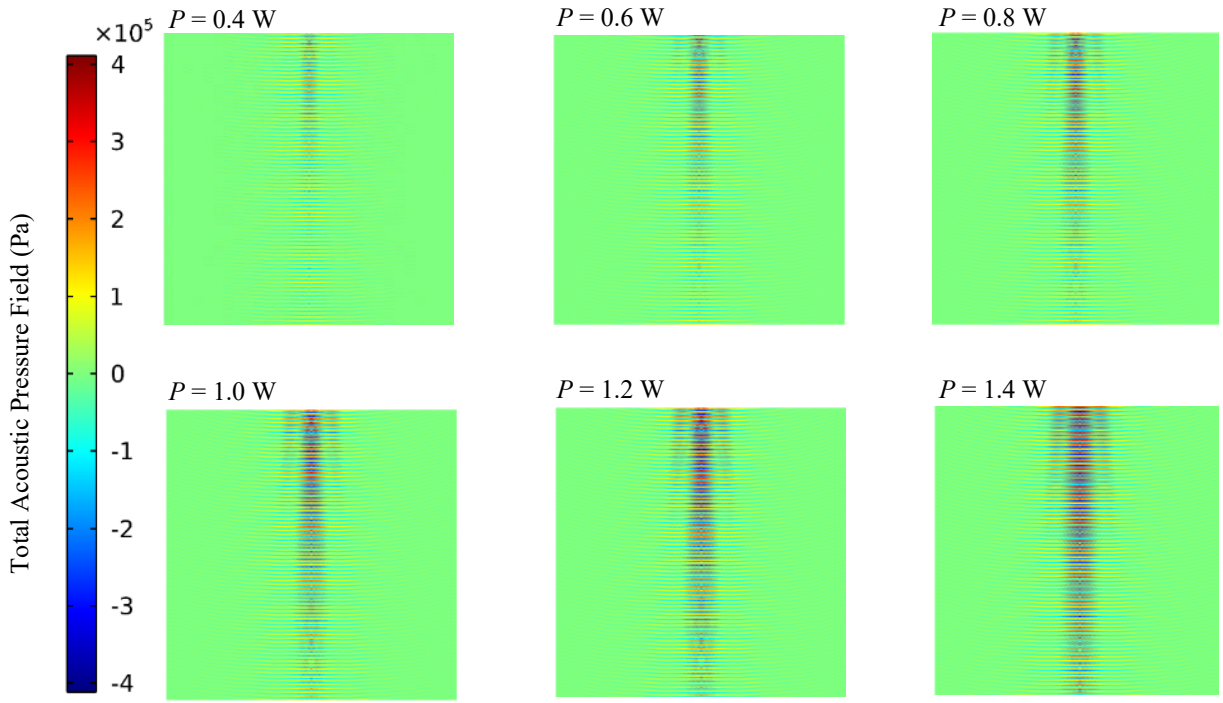


Figure 8. Simulated acoustic pressure distribution within tissues at t = 5 min for different transducer power levels, predicted by the numerical model.

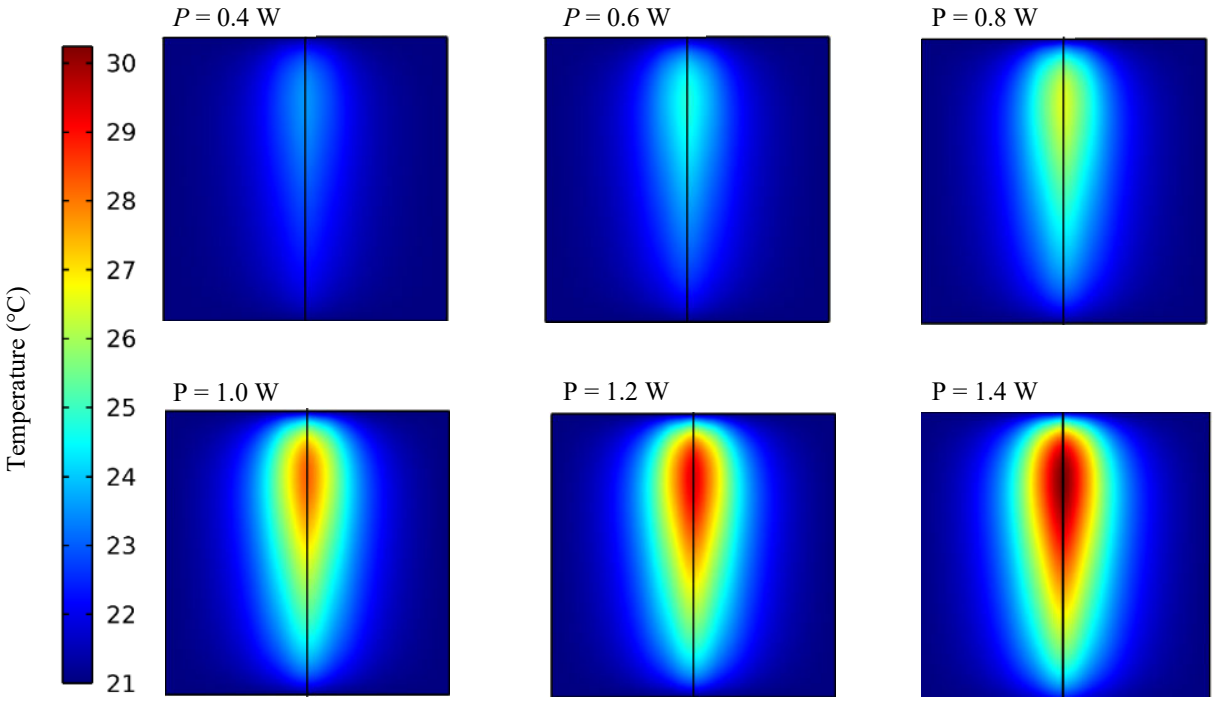


Figure 9. Simulated temperature distribution within tissues at t = 5 min for different transducer power levels, predicted by the coupled acoustic–thermal numerical model.

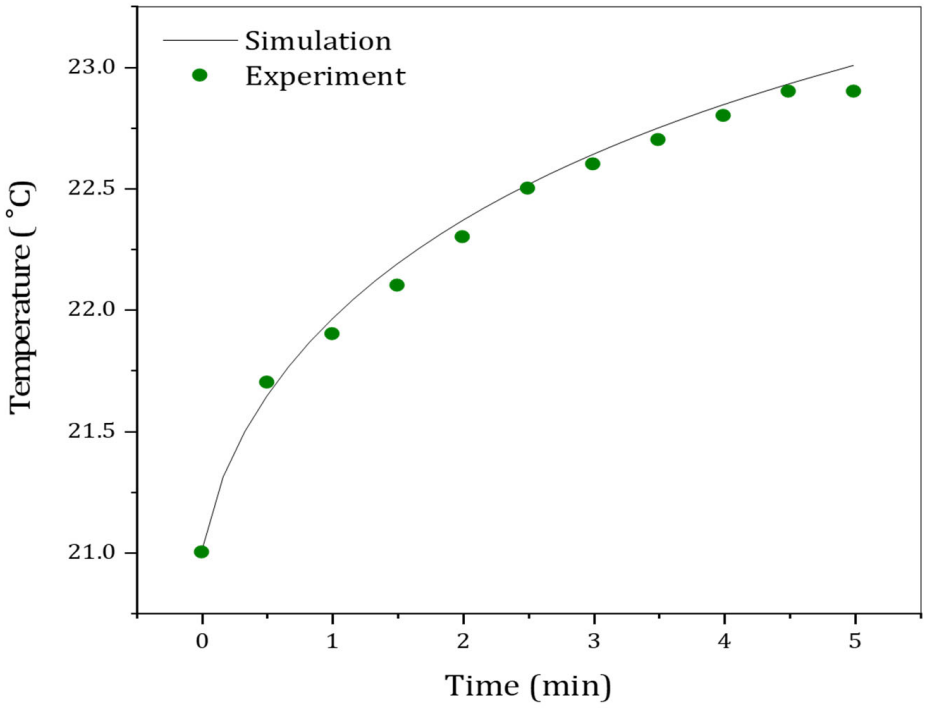


Figure 10. Comparison of the time-dependent temperature of the center of the tissue obtained from the numerical simulation and from the experiment.

4. Discussions

In order to achieve an appropriate treatment plan, a good understanding of the parameters involved in heat generation within tissues and the targeted tissue temperature is necessary. This study investigates some of the essential aspects of good ultrasound therapy, such as evaluating the effect of acoustic power on temperature rise in tissues, temperature differences between central and surrounding regions of the tissue during treatment, and

temperature gradients as a function of time during radiation. The main aim of the study was to control unwanted damage to the surrounding tissue, as monitoring inflammatory responses during ultrasound therapy is one of the biggest challenges in the field.

It should be noted that the present experimental setup employed a flat and unfocused ultrasound transducer rather than a clinically used focused HIFU transducer. Therefore, the current model does not fully reproduce the highly localized focal energy deposition observed in clinical HIFU systems. Instead, the aim of this study was to investigate the fundamental thermal behavior, temperature gradients, and heat transfer mechanisms generated by continuous therapeutic ultrasound exposure under controlled experimental conditions. Despite this limitation, the obtained findings provide useful insight into thermal distribution patterns and the potential risk of unwanted heating in surrounding tissues, which are relevant to ultrasound-based hyperthermia applications. Future studies should investigate focused transducer geometries and fully developed HIFU systems to improve clinical translation of the results. Furthermore, because the present study employed homogeneous ex vivo tissue and neglected physiological factors, such as blood perfusion and metabolic heat generation, the findings should be interpreted as fundamental thermal observations rather than direct predictions of in vivo clinical outcomes.

Insufficient attention to tissue temperature during treatment modalities is often connected with parallel damage to healthy tissues, hindering the practical application of ultrasound therapy in clinical practice. Particularly in hyperthermia, rises in temperature have to occur within the targeted tissues specifically. In contrast, neighboring tissues are allowed to have temperatures during exposure that do not cause thermal damage [64].

There was a significant difference between T_C and T_S in this study. This difference in clinical practice can be translated into a different thermal response in the deep regions of tissues during exposure. In cases of exposure with high intensities, equal attention must be paid to both T_S and T_C values to prevent unwanted damage to deep tissues. Moreover, the effect of increasing the power of the transducer on T_C was shown to be more significant than on T_S. This could be good news, as it means that the central cells are being killed, while the surrounding ones are protected from overheating. However, it should not be ignored that it is also equivalent to creating a more non-uniform temperature profile within the tissue. The importance of this issue may become greater in thicker or more structurally complex biological tissues, where acoustic attenuation and heterogeneous tissue properties can influence the spatial distribution of deposited thermal energy. In hyperthermia therapy, achieving a final uniform temperature profile is of high importance, as non-uniform temperature distributions change the geometry of the tissue into more complex shapes, making it more resistant to treatment. However, these data should be interpreted with caution, as practical treatments usually contain tissues with capillaries where the possible effects of blood flow on thermal convection cannot be ruled out [65,66]. Moreover, perfusion rate can also increase as the temperature of the tissue increases [67]. In addition to this, the amount of the temperature rise can also be influenced by the initial temperature of the tissue [68]. So, further tests with various initial temperatures should be undertaken before making any judgements. In addition, the present study was primarily designed to investigate thermal trends and to evaluate the agreement between experimental measurements and numerical predictions under different acoustic power levels. Although three independent tissue samples were evaluated for each power condition, the relatively limited number of replicates restricts the extent of statistical characterization that can be performed. Consequently, the reported temperatures should be interpreted primarily as representative thermal trends and comparative observations within the investigated experimental conditions.

Previous studies have demonstrated that pre-focal point temperature always has higher values than post-focal point temperature [69]. However, temperature monitoring and control of superficial injuries are by far easier than deep tissue damage. Superficial thermal injuries can be reduced using local ice compression to lower the temperature and prevent rapid temperature elevation due to the ultrasound energy accumulation at the skin surface.

5. Conclusions

In this study, the recorded temperatures from the central point and deep tissue during continuous irradiation of 3 MHz ultrasound waves at powers of 0.4 to 1.4 W were compared. But the main focus was the central point and surface point temperatures of the tissues, as these areas are hard to access with commonly used experimental techniques; thus, their temperature measurement is challenging. A proper understanding of temperature changes in deep tissues, particularly within internal organs, is essential for ultrasound therapy. Temperature distribution in tissues is dependent on exposure time, beam frequency, and the tissue attenuation coefficient; for each, a relevant experiment must be carried out to determine its role in the final outcome of hyperthermia therapy. Moreover, changes in the temperature within tissue is also influenced by internal parameters, such as tissue heat conductivity, blood circulation, and the normal baseline body temperature.

Experimental and numerical investigation of the role of blood vessels in the ultrasound therapy process demonstrated that blood flow could conserve the core tissue temperature [70], which should be considered during clinical ultrasound.

The present findings should be interpreted within the limitations of the study. The experiments were performed on homogeneous ex vivo chicken breast tissue using a flat, unfocused ultrasound transducer, and the numerical model neglected blood perfusion and metabolic heat generation. Consequently, the reported temperature distributions should not be directly extrapolated to clinical ultrasound therapy without further validation using physiologically representative tissue models and clinically relevant focused ultrasound systems.

Supplementary Materials: The following supporting information can be downloaded at: https://www.mdpi.com/article/10.3390/biophysica6040054/s1, Figure S1: Mean temperature rise at TC and TS for all investigated acoustic power levels.

Author Contributions: Conceptualization, A.D.; methodology, A.D.; software, A.D.; validation, A.D.; formal analysis, A.D. and P.J.; investigation, A.D.; resources, A.D.; data curation, A.D.; writing—original draft preparation, A.D. and M.S. and P.J.; writing—review and editing, A.D. and M.S. and P.J.; visualization, A.D.; supervision, A.D. and M.S.; project administration, A.D.; funding acquisition, A.D. All authors have read and agreed to the published version of the manuscript.

Funding: This work was supported by internal funding from the Hirszfeld Institute of Immunology and Experimental Therapy, Polish Academy of Sciences (HIIET PAS).

Data Availability Statement: The original contributions presented in this study are included in the article/Supplementary Materials. Further inquiries can be directed to the corresponding authors.

Acknowledgments: This project was conducted at the department of medical physics at Iran University of Medical Sciences (IUMS).

Conflicts of Interest: The authors declare that they have no known competing financial interests or personal relationships that could have appeared to influence the work reported in this paper.

References

1. Dahaghin, A.; Emadiyanrazavi, S.; Salimibani, M.; Bahreinizad, H.; Haghpanahi, M.; Eivazzadeh-keihan, R. A numerical investigation into the magnetic nanoparticles hyperthermia cancer treatment injection strategies. *Biocybern. Biomed. Eng.* **2021**, *41*, 516–526. [CrossRef]
2. Simon, C.; VanBaren, P.; Ebbini, E.S. Two-dimensional temperature estimation using diagnostic ultrasound. *IEEE Trans. Ultrason. Ferroelectr. Freq. Control* **1998**, *45*, 1088–1099. [CrossRef] [PubMed]
3. Dahaghin, A.; EmadiyanRazavi, S.; Tara, A.; Yashar, F.-M.; Maryam, M.M.; Changizi, V. *Cancer Treatment with Ultrasound*; Arshadan: Tehran, Iran, 2019.
4. Ohwatashi, A.; Ikeda, S.; Harada, K.; Kamikawa, Y.; Yoshida, A.; Inoue, K.; Yanagida, N.; Fukudome, K.; Kiyama, R.; Ohshige, T.; et al. Temperature changes caused by the difference in the distance between the ultrasound transducer and bone during 1 mhz and 3 mhz continuous ultrasound: A phantom study. *J. Phys. Ther. Sci.* **2015**, *27*, 205–208. [CrossRef] [PubMed]
5. Krasinski, D.; Thrasher, A.B.; Miller, M.G.; Holcomb, W.R. Effects of Transducer Mass on Intramuscular Temperature During Ultrasound Treatments. *J. Sport. Rehabil.* **2013**, *22*, 296–300. [CrossRef] [PubMed]
6. Miller, M.G.; Longoria, J.R.; Cheatham, C.C.; Baker, R.J.; Michael, T.J. Intramuscular temperature differences between the mid-point and peripheral effective radiating area with ultrasound. *J. Sports Sci. Med.* **2008**, *7*, 286. [PubMed]
7. Merrick, M.A.; Mihalyov, M.R.; Roethemeier, J.L.; Cordova, M.L.; Ingersoll, C.D. A comparison of intramuscular temperatures during ultrasound treatments with coupling gel or gel pads. *J. Orthop. Sports Phys. Ther.* **2002**, *32*, 216–220. [CrossRef] [PubMed]
8. Yoshizawa, S.; Ikeda, T.; Ito, A.; Ota, R.; Takagi, S.; Matsumoto, Y. High intensity focused ultrasound lithotripsy with cavitating microbubbles. *Med. Biol. Eng. Comput.* **2009**, *47*, 851–860. [CrossRef] [PubMed]
9. Mitragotri, S. Healing sound: The use of ultrasound in drug delivery and other therapeutic applications. *Nat. Rev. Drug Discov.* **2005**, *4*, 255–260. [CrossRef] [PubMed]
10. Sirsi, S.R.; Borden, M.A. State-of-the-art materials for ultrasound-triggered drug delivery. *Adv. Drug Deliv. Rev.* **2014**, *72*, 3–14. [CrossRef] [PubMed]
11. Samimi, S.; Maghsoudnia, N.; Eftekhari, R.B.; Dorkoosh, F. Lipid-Based Nanoparticles for Drug Delivery Systems. In *Characterization and Biology of Nanomaterials for Drug Delivery*; Elsevier: Amsterdam, The Netherlands, 2019; pp. 47–76. [CrossRef]
12. Ting, C.-Y.; Fan, C.-H.; Liu, H.-L.; Huang, C.-Y.; Hsieh, H.-Y.; Yen, T.-C.; Wei, K.C.; Yeh, C.K. Concurrent blood–brain barrier opening and local drug delivery using drug-carrying microbubbles and focused ultrasound for brain glioma treatment. *Biomaterials* **2012**, *33*, 704–712. [CrossRef] [PubMed]
13. Aryal, M.; Arvanitis, C.D.; Alexander, P.M.; McDannold, N. Ultrasound-mediated blood–brain barrier disruption for targeted drug delivery in the central nervous system. *Adv. Drug Deliv. Rev.* **2014**, *72*, 94–109. [CrossRef] [PubMed]
14. Taloub, S.; Hobar, F.; Astefanoaei, I.; Dumitru, I.; Caltun, O.F. FEM Investigation of coated magnetic nanoparticles for hyperthermia. *Nanosci. Nanotechnol.* **2016**, *6*, 55–61. [CrossRef]
15. Dahaghin, A.; Emadiyanrazavi, S.; Haghpanahi, M.; Salimibani, M.; Bahreinizad, H.; Eivazzadeh-Keihan, R.; Maleki, A. A comparative study on the effects of increase in injection sites on the magnetic nanoparticles hyperthermia. *J. Drug Deliv. Sci. Technol.* **2021**, *63*, 102542. [CrossRef]
16. Lee, K.I. Prediction and Measurement of Temperature Rise Induced by High Intensity Focused Ultrasound in a Tissue-Mimicking Phantom. *J. Korean Phys. Soc.* **2018**, *72*, 1313–1319. [CrossRef]
17. Namakshenas, P.; Mojra, A. Numerical study of non-Fourier thermal ablation of benign thyroid tumor by focused ultrasound (FU). *Biocybern. Biomed. Eng.* **2019**, *39*, 571–585. [CrossRef]
18. Ritchie, R.W.; Leslie, T.; Phillips, R.; Wu, F.; Illing, R.; Ter Haar, G.; Protheroe, A.; Cranston, D. Extracorporeal high intensity focused ultrasound for renal tumours: A 3-year follow-up. *BJU Int.* **2010**, *106*, 1004–1009. [CrossRef] [PubMed]
19. Tourinho-Barbosa, R.R.; Sanchez-Salas, R.; Claros, O.R.; Collura-Merlier, S.; Bakavicius, A.; Carneiro, A.; Stabile, A.; Moschini, M.; Cathala, N.; Tobias-Machado, M.; et al. Focal therapy for localized prostate cancer with either high intensity focused ultrasound or cryoablation: A single institution experience. *J. Urol.* **2020**, *203*, 320–330. [CrossRef] [PubMed]
20. Ma, B.; Liu, X.; Yu, Z. The effect of high intensity focused ultrasound on the treatment of liver cancer and patients' immunity. *Cancer Biomark.* **2019**, *24*, 85–90. [CrossRef] [PubMed]
21. Abe, S.; Osada, T.; Kaneko, K.; Zhong, P.; Lyerly, H.K. A novel combination therapy of high intensity focused ultrasound and PDL1 blockades against advanced breast cancer. *Cancer Res.* **2019**, *79*, 4071. [CrossRef]
22. Varano, G.M.; Mauri, G.; Mascagni, L.; Della Vigna, P.; Bonomo, G.; Maiettini, D.; Orsi, F. High-Intensity Focused Ultrasound Ablation of Pancreatic Cancer. *Dig. Dis. Interv.* **2019**, *3*, 243–252. [CrossRef]
23. Keshavarzi, A.; Vaezy, S.; Noble, M.L.; Chi, E.Y.; Walker, C.; Martin, R.W.; Fujimoto, V.Y. Treatment of uterine leiomyosarcoma in a xenograft nude mouse model using high-intensity focused ultrasound: A potential treatment modality for recurrent pelvic disease. *Gynecol. Oncol.* **2002**, *86*, 344–350. [CrossRef]
24. Zeinali, B.; Mojra, A.; Vafai, K. A genetically optimized physics-informed neural network for multiphysics modeling of magnetic hyperthermia in brain cancer. *Comput. Biol. Med.* **2026**, *206*, 111621. [CrossRef] [PubMed]

25. Izadifar, Z.; Babyn, P.; Chapman, D. Mechanical and biological effects of ultrasound: A review of present knowledge. *Ultrasound Med. Biol.* **2017**, *43*, 1085–1104. [CrossRef] [PubMed]
26. Einolghasi, F.B.; Zeinali, B.; Vafai, K.; Mojra, A. Development of a prediction model for hyperthermia-enhanced drug delivery using thermosensitive nanoparticles. *J. Therm. Biol.* **2025**, *129*, 104124. [CrossRef] [PubMed]
27. Rao, W.; Deng, Z.-S. A review of hyperthermia combined with radiotherapy/chemotherapy on malignant tumors. *Crit. Rev. Biomed. Eng.* **2010**, *38*, 101–116. [CrossRef] [PubMed]
28. Maraghechi, B.; Kolios, M.C.; Tavakkoli, J.; Hasani, M.H. Temperature dependence of harmonics generated by nonlinear ultrasound beam propagation in water: A simulation study. In Proceedings of the 2014 IEEE International Ultrasonics Symposium, Chicago, IL, USA, 3–6 September 2014; pp. 1456–1459. [CrossRef]
29. Suleman, M.; Riaz, S. 3D in silico study of magnetic fluid hyperthermia of breast tumor using Fe_3O_4 magnetic nanoparticles. *J. Therm. Biol.* **2020**, *91*, 102635. [CrossRef] [PubMed]
30. Kumar, P.; Kumar, D.; Rai, K.N. A numerical study on dual-phase-lag model of bio-heat transfer during hyperthermia treatment. *J. Therm. Biol.* **2015**, *49*, 98–105. [CrossRef] [PubMed]
31. Jung, S.E.; Cho, S.H.; Jang, J.H.; Han, J.-Y. High-intensity focused ultrasound ablation in hepatic and pancreatic cancer: Complications. *Abdom. Imaging* **2011**, *36*, 185–195. [CrossRef] [PubMed]
32. Maleki, A. Green oxidation protocol: Selective conversions of alcohols and alkenes to aldehydes, ketones and epoxides by using a new multiwall carbon nanotube-based hybrid nanocatalyst via ultrasound irradiation. *Ultrason. Sonochem.* **2018**, *40*, 460–464. [CrossRef] [PubMed]
33. Luan, S.; Zhou, H.; Ni, X.; Zhu, B. Thermal response predication for complex biological tissues subjected to high intensity focused ultrasound. *Ultrasonics* **2026**, *164*, 108013. [CrossRef] [PubMed]
34. Dahaghin, A.; Salimibani, M.; Jahansa, P.; Shiran, M.B.; Bahreinizad, H.; Haghpanahi, M.; Maleki, A. Evaluation of the Accuracy from Thermal Imaging Results in Experimental Tests When Using 1 MHZ Therapeutic Ultrasound. *SSRN Electron. J.* **2024**. [CrossRef]
35. Karwat, P.; Kujawska, T.; Lewin, P.A.; Secomski, W.; Gambin, B.; Litniewski, J. Determining temperature distribution in tissue in the focal plane of the high (>100 W/cm^2) intensity focused ultrasound beam using phase shift of ultrasound echoes. *Ultrasonics* **2016**, *65*, 211–219. [CrossRef] [PubMed]
36. Lu, X.; Sankin, G.; Pua, E.C.; Madden, J.; Zhong, P. Activation of transgene expression in skeletal muscle by focused ultrasound. *Biochem. Biophys. Res. Commun.* **2009**, *379*, 428–433. [CrossRef] [PubMed]
37. Rwei, P.; Gong, C.-S.A.; Luo, L.-J.; Lin, M.-B.; Lai, J.-Y.; Liu, H.-L. In vitro investigation of ultrasound-induced oxidative stress on human lens epithelial cells. *Biochem. Biophys. Res. Commun.* **2017**, *482*, 954–960. [CrossRef] [PubMed]
38. Tsui, P.; Shu, Y.; Chen, W.; Liu, H.; Hsiao, I.; Chien, Y. Ultrasound temperature estimation based on probability variation of backscatter data. *Med. Phys.* **2012**, *39*, 2369–2385. [CrossRef] [PubMed]
39. Dalecki, D. Mechanical bioeffects of ultrasound. *Annu. Rev. Biomed. Eng.* **2004**, *6*, 229–248. [CrossRef] [PubMed]
40. Georg, O.; Wilkens, V. Non-invasive estimation of temperature using diagnostic ultrasound during hifu therapy. *AIP Conf. Proc.* **2017**, *1816*, 40002. [CrossRef]
41. Gas, P.; Miaskowski, A.; Dobrowolski, D. Modelling the tumor temperature distribution in anatomically correct female breast phantom. *Prz. Elektrotechniczny* **2020**, *96*, 146–149. [CrossRef]
42. Samanipour, R.; Maerefat, M.; Nejad, H.R. Numerical study of the effect of ultrasound frequency on temperature distribution in layered tissue. *J. Therm. Biol.* **2013**, *38*, 287–293. [CrossRef]
43. Maqbool, M. *An Introduction to Medical Physics*; Springer: Berlin/Heidelberg, Germany, 2017. [CrossRef]
44. Schmickl, C.N.; Menon, A.A.; Dhokarh, R.; Seth, B.; Schembri, F. Optimizing B-lines on lung ultrasound: An in-vitro to in-vivo pilot study with clinical implications. *J. Clin. Monit. Comput.* **2019**, *34*, 277–284. [CrossRef] [PubMed]
45. Ng, A.; Swanevelder, J. Resolution in ultrasound imaging. *Contin. Educ. Anaesth. Crit. Care Pain.* **2011**, *11*, 186–192. [CrossRef]
46. Buniyamin, N.; Halim, M.H.A. Adjusting Time of Flight in Ultrasound B-mode Imaging for Accurate Measurement of Fat using Image Segmentation Technique. *J. ICT Res. Appl.* **2017**, *11*, 1–20. [CrossRef]
47. Sarvazyan, A.; Tsyuryupa, S. Potential biomedical applications of non-dissipative acoustic radiation force. *Proc. Meet. Acoust.* **2016**, *26*, 20002. [CrossRef]
48. Greenspan, M.; Tschiegg, C.E. Speed of sound in water by a direct method. *J. Res. Natl. Bur. Stand.* **1957**, *59*, 249–254. [CrossRef]
49. Adams, M.T.; Cleveland, R.O.; Roy, R.A. Modeling-based design and assessment of an acousto-optic guided high-intensity focused ultrasound system. *J. Biomed. Opt.* **2017**, *22*, 17001. [CrossRef] [PubMed]
50. Yetik, H.; Ariyurek, C.; Bozkurt, A.; Ergun, A.S. Frequency optimization in high intensity focused ultrasound. In Proceedings of the 2014 IEEE International Ultrasonics Symposium, Chicago, IL, USA, 3–6 September 2014; pp. 409–412. [CrossRef]
51. Hynynen, K. Biophysics and technology of ultrasound hyperthermia. In *Methods of External Hyperthermic Heating*; Springer: Berlin/Heidelberg, Germany, 1990; pp. 61–115. [CrossRef]

52. Huang, H.-W.; Hui, L.; Chen, Y.-H.; Cheng, Y.H. A Computational Investigation of Atrial Fibrillation Treatment Using HIFU Energy Source. 2019. Available online: https://teacher.tku.edu.tw/StfFdDtl.aspx?tid=7004937 (accessed on 16 April 2026).
53. Abdolhosseinzadeh, A.; Mojra, A.; Hooman, K. A porous medium approach to thermal analysis of focused ultrasound for treatment of thyroid nodules. *Appl. Acoust.* **2021**, *182*, 108236. [CrossRef]
54. Khanghahi-Bala, B.; Habibagahi, G.; Ghabezloo, S.; Ghahramani, A.; Schrefler, B.A. Heat generation by ultrasound wave propagation in porous media with low permeability: Theoretical framework and coupled numerical modeling. *Comput. Geotech.* **2020**, *124*, 103607. [CrossRef]
55. Pennes, H.H. Analysis of Tissue and Arterial Blood Temperatures in the Resting Human Forearm. *J. Appl. Physiol.* **1998**, *85*, 5–34. [CrossRef] [PubMed]
56. Singh, N. Advanced computational approaches for bioheat transfer in minimally invasive cancer thermal therapies. *Front. Therm. Eng.* **2026**, *6*, 1798897. [CrossRef]
57. Solovchuk, M.; Sheu, T.W.H.; Thiriet, M. Simulation of nonlinear Westervelt equation for the investigation of acoustic streaming and nonlinear propagation effects. *J. Acoust. Soc. Am.* **2013**, *134*, 3931–3942. [CrossRef] [PubMed]
58. Parmar, N.; Kolios, M.C. An investigation of the use of transmission ultrasound to measure acoustic attenuation changes in thermal therapy. *Med. Biol. Eng. Comput.* **2006**, *44*, 583–591. [CrossRef] [PubMed]
59. Dahaghin, A.; Salimibani, M.; Boszczyk, A.; Jóźwik, A.; Grasa, J.; Przeździecka-Dołyk, J.; Siedlecki, D. Biomechanical simulations of crystalline lens oscillations resulting from the changes in the gaze in an accommodated eye. *Front. Bioeng. Biotechnol.* **2025**, *13*, 1504769. [CrossRef] [PubMed]
60. Azhari, H. *Basics of Biomedical Ultrasound for Engineers*; John Wiley & Sons: Hoboken, NJ, USA, 2010. [CrossRef]
61. Li, C.; Miao, J.; Yang, K.; Guo, X.; Tu, J.; Huang, P.; Zhang, D. Fourier and non-Fourier bio-heat transfer models to predict ex vivo temperature response to focused ultrasound heating. *J. Appl. Phys.* **2018**, *123*, 174906. [CrossRef]
62. Yang, X.; Jo, J. Enhanced cavitation by using two consecutive ultrasound waves at different frequencies. *Appl. Phys. Lett.* **2014**, *105*, 193701. [CrossRef] [PubMed]
63. Fan, P.; Yin, C.; Xue, H.; Xie, L.; Sun, W.; Tu, J.; Guo, X.; Kong, X.; Zhang, D. In vivo evaluation of two-dimensional temperature variation in perirenal fat of pigs with B-mode ultrasound. *J. Appl. Phys.* **2019**, *126*, 84902. [CrossRef]
64. Bakker, A.; Kolff, M.W.; Holman, R.; van Leeuwen, C.M.; Korshuize-van Straten, L.; de Kroon-Oldenhof, R.; Rasch, C.R.; van Tienhoven, G.; Crezee, H. Thermal skin damage during reirradiation and hyperthermia is time-temperature dependent. *Int. J. Radiat. Oncol. Biol. Phys.* **2017**, *98*, 392–399. [CrossRef] [PubMed]
65. Etminan, A.; Dahaghin, A.; Emadiyanrazavi, S.; Bani, M.S.; Eivazzadeh-Keihan, R.; Haghpanahi, M.; Maleki, A. Simulation of heat transfer, mass transfer and tissue damage in magnetic nanoparticle hyperthermia with blood vessels. *J. Therm. Biol.* **2022**, *110*, 103371. [CrossRef] [PubMed]
66. Etminan, A.; Salimibani, M.; Dahaghin, A.; Haghpanahi, M.; Maleki, A. FEM thermal assessment of a 3-D irregular tumor with capillaries in magnetic nanoparticle hyperthermia via dissimilar injection points. *Comput. Biol. Med.* **2023**, *157*, 106771. [CrossRef] [PubMed]
67. Kok, H.P.; Van Haaren, P.M.A.; Van Dijk, J.D.P.; Crezee, J. On estimation of the temperature maximum in intraluminal or intracavitary hyperthermia. *Int. J. Hyperth.* **2009**, *21*, 287–304. [CrossRef] [PubMed]
68. Bielas, R.; Bochińska, A.; Józefczak, A. The influence of initial temperature on ultrasonic hyperthermia measurements. *Appl. Acoust.* **2020**, *164*, 107259. [CrossRef]
69. Zhou, Y.; Wilson Gao, X. Variations of bubble cavitation and temperature elevation during lesion formation by high-intensity focused ultrasound. *J. Acoust. Soc. Am.* **2013**, *134*, 1683–1694. [CrossRef] [PubMed]
70. Kooiman, K.; Roovers, S.; Langeveld, S.A.G.; Kleven, R.T.; Dewitte, H.; O'Reilly, M.A.; Escoffre, J.M.; Bouakaz, A.; Verweij, M.D.; Hynynen, K.; et al. Ultrasound-responsive cavitation nuclei for therapy and drug delivery. *Ultrasound. Med. Biol.* **2020**, *46*, 1296–1325. [CrossRef] [PubMed]

Disclaimer/Publisher's Note: The statements, opinions and data contained in all publications are solely those of the individual author(s) and contributor(s) and not of MDPI and/or the editor(s). MDPI and/or the editor(s) disclaim responsibility for any injury to people or property resulting from any ideas, methods, instructions or products referred to in the content.